NJC

Accepted Manuscript

1　　**A highly selective turn-on fluorescent sensor for fluoride and its application in imaging of**

2　　**living cells**

3　　Jiun-Ting Yeh, Parthiban Venkatesan, Shu-Pao Wu*

4　　Department of Applied Chemistry, National Chiao Tung University, Hsinchu, Taiwan 300,

5　　Republic of China

6
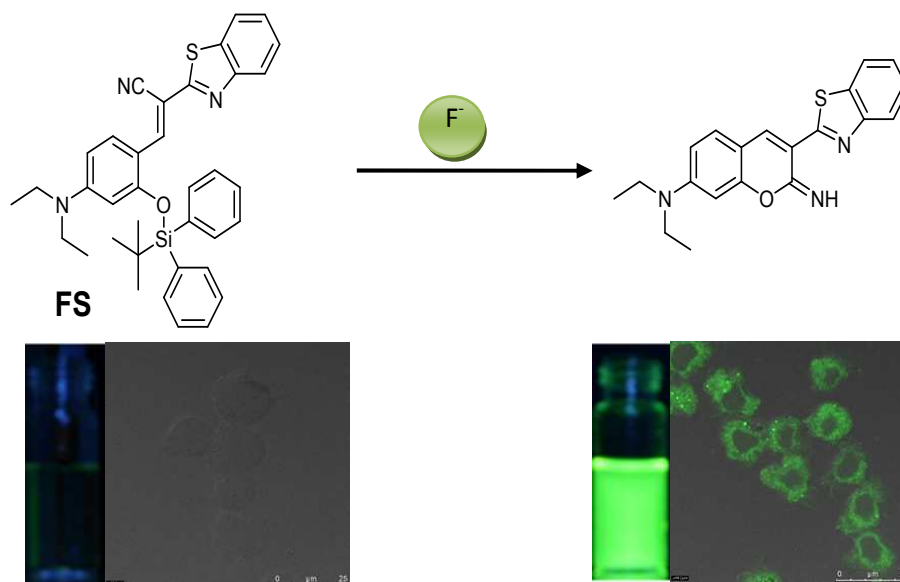
7

8

9

10　　∗ Corresponding author. Tel.: +886-3-5712121-ext 56506; fax: +886-3-5723764; e-mail:

11　　spwu@mail.nctu.edu.tw

12

13

14

15

16

1

17 **Abstract**

18 A fluorescent probe (**FS**) based on a fluoride-specific desilylation reaction has been developed

19 for highly selective and sensitive detection of F$^-$. In the presence of F$^-$, the probe **FS** provided

20 significant green fluorescence enhancement, while other anions produced only minor changes in

21 fluorescence intensity. The probe **FS** has a limit of detection of 1.45 μM, which is reasonable for

22 the detection of micromolar concentrations of F$^-$ ion. The maximum fluorescence enhancement

23 induced by F$^-$ in the probe was observed over the pH range 7–10. Moreover, fluorescence

24 microscopy imaging using mouse leukaemic monocyte macrophage showed that the probe **FS**

25 could be an efficient fluorescent probe for F$^-$ ions in living cells.

26

28

29

30

31

32

33

34

35

36

37

38

39

1. Introduction

The development of sensors for biologically important anions is currently an important research focus because of their important roles in various biological processes.[1-5] Fluoride is a useful additive in toothpaste and in drinking water for the prevention of dental caries. However, excess fluoride can result in fluorosis, urolithiasis, and cancer.[6-11] Therefore, precise determination of fluoride in samples is necessary. Up to now, several methods such as ion chromatography,[12,13] ion-selective electrode,[14] and the Willard and Winter methods[15] have been used for quantitative fluoride detection. On the other hand, these methods have some disadvantages such as high costs and complicated procedures. Now, more attention has focused on the development of highly selective and convenient methods for fluoride detection.

A large number of fluorescent probes have been developed for fluoride detection based on three molecular interactions: hydrogen bonding between fluoride and NH hydrogen (amide, indole, pyrrole, thiourea, and urea),[16-26] boron–fluoride complexation[27-30], and fluoride-mediated desilylation[31-35]. Because fluoride ions have strong tendency for hydration, the approach using hydrogen bonding is not applicable in aqueous media. Fluoride-mediated desilylation strategy does not have such limitation and can provide the best way for detecting fluoride in aqueous solution. In this study, a coumarin derivative with Si–O functionality was used for the detection of fluoride anion in living cells.

In this study, we designed a fluorescent chemosensor **FS** for fluoride detection. The chemosensor comprises two parts: a Si–O functionality and a coumarin derivative. F^- triggers cleavage of the Si–O bond, leading to formation of the strong green emission of the coumarin derivative. We have performed a competitive analysis for F^- ions with other anions such as Br^-, CN^-, Cl^-, $H_2PO_4^-$, I^-, NO_2^-, NO_3^-, N_3^-, OAc^-, and $P_2O_7^{4-}$ with **FS**. The result shows that F^- is

63   the only anion that triggers the cleavage of the Si–O bond in **FS** and that it causes formation of a

64   strongly fluorescent green derivative while other anions do not. This new probe exhibits high

65   selectivity and sensitivity toward F^- over other anions in aqueous solutions. Most importantly,

66   **FS** shows good permeability for cell membranes and is applicable to F^- imaging of living cells.

67   **2. Experimental section**

68   **2.1 Materials and Instrumentation.**

69   All solvents and reagents were obtained from commercial sources and used as received without

70   further purification. UV/Vis spectra were recorded on an Agilent 8453 UV/Vis spectrometer.

71   NMR spectra were obtained on a Bruker DRX-300 and Agilent Unity INOVA-500 NMR

72   spectrometer. IR data were obtained on Bomem DA8.3 Fourier-Transform Infrared Spectrometer.

73   Fluorescence spectra measurements were performed on a Hitachi F-7000 Fluorescence

74   spectrophotometer. Fluorescent images were taken on a Leica TCS SP5 X AOBS Confocal

75   Fluorescence Microscope.

76   **2.2 Synthesis of 2-((tert-butyldiphenylsilyl)oxy)-4-(diethylamino)benzaldehyde (1)**

77   4-Diethylaminosalicyl aldehyde (193 mg, 1.00 mmol), imidazole (100 mg，1.47 mmol) and

78   tert-butyldiphenylchlorosilane (275 µL, 1.0 mmol) were dissolved in DMF (1 mL). The mixture

79   was stirred at 50 ^{o}C for 12 hr. The solvent was removed under reduced pressure, and the crude

80   product was purified by column chromatography (hexane: ethyl acetate = 4:1) to give the

81   compound as a white solid. Yield: 384 mg (89.2%). Melting point: 108~109 ^{o}C. ^{1}H-NMR (300

82   MHz, CDCl$_3$): δ 10.49 (s, 1 H), 7.77-7.78 (m, 5 H), 7.37-7.44 (m, 6 H), 6.22 (d, J = 9.0 Hz, 1 H),

83   5.59 (s, 1 H), 2.93 (q, J = 6.6 Hz, 4H), 1.13 (s, 9 H), 0.76 (t, J = 6.9 Hz, 6 H); ^{13}C-NMR (125

84   MHz, CDCl$_3$): δ 187.2, 160.8, 153.1, 135.3, 132.3, 130.0, 129.8, 127.9, 115.6, 105.2, 100.9, 44.4,

85   26.5, 19.6, 12.1. MS (EI): m/z (%) = 431 (6.4), 374 (100), 354 (1.7), 330 (12.9), 224 (2.1);

86   HRMS (EI): calcd for $C_{36}H_{37}N_3OSSi$ (M^+) 431.2281; found, 431.2277.

87   **2.3 Synthesis of (E)-2-(benzo[d]thiazol-2-yl)-3-(2-((tert-butyldiphenylsilyl)oxy)-**

88   **4-(diethylamino)phenyl)acrylonitrile (FS)**

89   To the solution of 1,3-benzothiazol-2-ylacetonitrile (87 mg，0.5 mmol) dissolved in 10 mL

90   methanol, piperidine (150 μL) was added and stirred for 5 min. 2-((tert-Butyldiphenylsilyl)oxy)-

91   4-(diethylamino)benzaldehyde was added to the mixture, and stirred at room temperature

92   overnight. An orange precipitate was formed, and the crude product was filtered, and thoroughly

93   washed with methanol to give the compound **FS**. Yield, 41 mg (14.0 %). Melting point: 197~198

94   ^{o}C. ^{1}H-NMR (300 MHz, CDCl$_3$): δ 8.88 (s, 1 H), 8.49 (d, J = 9.3 Hz, 1 H), 8.03 (d, J = 8.1 Hz, 1

95   H), 7.87 (d, J = 7.8 Hz, 1 H), 7.78-7.80 (m, 4 H), 7.34-7.51 (m, 8H), 6.33 (dd, J = 9.3 Hz, J = 1.8

96   Hz, 1 H), 5.70 (d, J = 1.8 Hz, 1 H), 2.98 (q, J = 6.9 Hz, 4H), 1.25 (s, 9 H) 0.80 (t, J = 7.2 Hz, 6

97   H); ^{13}C-NMR (125 MHz, CDCl$_3$): δ 165.9, 158.0, 154.0, 151.9, 141.5, 135.4, 134.3, 132.1, 130.2,

98   128.0, 126.3, 124.8, 122.9, 121.2, 118.5, 111.3, 105.9, 101.4, 96.1, 44.6, 26.7, 19.7, 12.3. IR

99   (KBr): 2969, 2927, 2854, 2212, 1609, 1591, 1559 cm^{-1}. MS (EI): m/z (%) = 587(97.3), 530(100);

100   HRMS (EI): calcd for $C_{36}H_{37}N_3OSSi$ (M^+) 587.2427; found, 587.2420.

101   **2.4 Anion selection study by fluorescence spectroscopy.** Chemosensor **FS** (10 μM) was added

102   with different aions (1 mM). All spectra were measured in 1.0 mL acetonitrile-water solution

103   (v/v = 1:1, 10 mM Hepes, pH 7.0). The light path length of cuvette was 1.0 cm.

104   **2.5 The pH dependence on the reaction of fluoride with chemosensor FS by fluorescence**

105   **spectroscopy.** Chemosensor **FS** (10 μM) was added with F$^-$ (20 μM) in 1.0 mL acetonitrile-

106   water solution (v/v = 1:1, 10 mM buffer). The buffers were: pH 3 ~ 4, KH$_2$PO$_4$/HCl; pH 4.5 ~ 6,

107   KH$_2$PO$_4$/NaOH; pH 6.5 ~ 8.5, HEPES; pH 9 ~ 10, Tris-HCl.

108   **2.6 Cell Culture**

109 RAW 264.7 cells were cultured in Dulbecco's modied Eagle's medium (DMEM)

110 supplemented with 10% fetal bovine serum (FBS) at 37 °C under an atmosphere of 5% CO2.

111 Cells were plated on 18 mm glass coverslips and allowed to adhere for 24 h.

112 **2.7 Cytotoxicity assay**

113 The methyl thiazolyl tetrazolium (MTT) assay was used to measure the cytotoxicity of **FS**

114 in RAW264.7 cells. RAW264.7 cells were seeded into a 96-well cell-culture plate. Various

115 concentrations (5, 10, 15, 20, 25 μM) of **FS** were added to the wells. The cells were incubated at

116 37°C under 5% CO_2 for 24 h. 10 μL MTT (5 mg/mL) was added to each well and incubated at

117 37°C under 5% CO_2 for 4 h. Remove the MTT solution and yellow precipitates (formazan)

118 observed in plates were dissolved in 200 μL DMSO and 25 μL Sorenson's glycine buffer (0.1 M

119 glycine and 0.1 M NaCl). Multiskan GO microplate reader was used to measure the absorbance

120 at 570 nm for each well. The viability of cells was calculated according to the following equation:

121 Cell viability (%) = (mean of absorbance value of treatment group) / (mean of absorbance value

122 of control group).

123 **2.8 Cell imaging**

124 Experiments to assess the F⁻ uptake were performed in phosphate-buffered saline (PBS)

125 with 20 μM NaF. The cells cultured in DMEM were treated with 10 mM solutions of NaF (2 μL;

126 final concentration: 20 μM) dissolved in sterilized PBS (pH = 7.4) and incubated at 37 °C for 30

127 min. The treated cells were washed with PBS (3×2 mL) to remove remaining metal ions. DMEM

128 (2 mL) was added to the cell culture, which was then treated with a 10 mM solution of

129 chemosensor **FS** (2 μL; final concentration: 20 μM) dissolved in DMSO. The samples were

130 incubated at 37 °C for 30 min. The culture medium was removed, and the treated cells were

131 washed with PBS (3×2 mL) before observation. Confocal fluorescence imaging of cells was

132 performed with a Leica TCS SP5 X AOBS Confocal Fluorescence Microscope (Germany), and a

133 63x oil-immersion objective lens was used. The cells were excited with a white light laser at 480

134 nm, and emission was collected at 535±10 nm.

135

136 **3. Results and discussion**

137 **3.1 Synthesis of the probe FS**

138 Synthesis of the probe **FS** is outlined in Scheme 1. 4-Diethylaminosalicyl aldehyde and tert-

139 butyldiphenylchlorosilane were reacted to form 2-((tert-butyldiphenylsilyl)oxy)-4-(diethylamino)

140 benzaldehyde. Further reaction of 2-((tert-butyldiphenylsilyl)oxy)-4-(diethylamino)

141 benzaldehyde with 1,3-benzothiazol-2-ylacetonitrile in equimolar quantities yields the

142 chemosensor **FS** (Scheme 1). **FS** is yellow and has an absorption band centered at 465 nm with a

143 quantum yield (Φ) of 0.001.

144 **3.2 Anion-sensing properties**

145 To evaluate the selectivity of the chemosensor **FS** toward various anions, absorption spectra

146 and fluorescence spectra of **FS** were measured in the presence of 12 anions: F^-, Br^-, Cl^-, CN^-,

147 $H_2PO_4^-$, HSO_3^-, I^-, N_3^-, NO_2^-, NO_3^-, OAc^-, and $P_2O_7^{4-}$ (Fig. 1). Only F^- caused a visible color

148 change in **FS** (yellow to green) and had a green emission (Fig. 1). Fig. 2 shows the absorption

149 spectra and fluorescence spectra of **FS** with various anions. Addition of F^- caused the absorption

150 band at 465 nm to shift to 483 nm and formation of a new emission band centered at 521 nm.

151 Fig. 3 shows the F^- titration with the chemosensor **FS**. After addition of 100 equivalents of F^-,

152 the emission intensity reached a maximum. The quantum yield of the new emission band was

153 0.146, which is 146-fold that of the chemosensor **FS** at 0.001. Fluoride ion was the only anion

154 that we tested that readily reacts with **FS** to yield a significant fluorescence enhancement,

155   suggesting application for the highly selective detection of F^- ion. The limit of detection for the

156   chemosensor **FS** as a fluorescent sensor for F^- detection was determined from a plot of

157   fluorescence intensity as a function of F^- concentration (see Fig. S7 in the supplementary data).

158   We found that the chemosensor **FS** has a limit of detection of 1.45 μM, which is reasonable for

159   the detection of micromolar concentrations of F^- ion.

160   The time course for the reaction of the chemosensor **FS** with fluoride is shown in Fig. 4.

161   The pseudo-first-order condition (10 μM **FS**, 1 mM F^-) was employed. By fitting the time course,

162   the observed rate constant for F^- deprotection of **FS** was found to be 0.0155 min^{-1}. The

163   mechanism of fluoride-mediated desilylation is shown in Scheme 2. F^- triggers cleavage of the

164   Si–O bond in **FS**, and then phenol attacks the cyano group to form a cyclic coumarin derivative

165   with strong green emission. To confirm the formation of the coumarin ring through the reaction

166   of **FS** with NaF, ^{1}H NMR spectroscopy (Fig. 5) was employed. After the reaction with F^-, the

167   imine proton (δ 8.88 ppm, H_d) of **FS** showed upfield shifts due to the formation of a cyclic

168   coumarin derivative. The proton signals (H_a and H_b) in the phenyl ring showed downfield shifts

169   after the reaction. These observations support the formation of the coumarin ring.

170   To study the influence of other anions on the reaction of F^- with the chemosensor **FS**, we

171   performed competitive experiments with other anions (1 mM) in the presence of F^- (1 mM)

172   (Fig. 6). The observed fluorescence enhancement for mixtures of F^- with most anions was

173   similar to that seen for F^- alone. We observed high fluorescence enhancement only with

174   mixtures of F^- with CN^- or $P_2O_7^{4-}$, indicating that CN^- and $P_2O_7^{4-}$ might aid the reaction of F^-

175   with the chemosensor **FS**. No other anions appeared to interfere with the fluorescence of the

176   chemosensor **FS** and F^-.

177   We performed pH titration of the chemosensor **FS** to investigate a suitable pH range for the

178   reaction of F⁻ with the chemosensor **FS**. As shown in Fig. 7, the emission intensities of the

179   chemosensor **FS** are very low. After mixing of **FS** with F⁻ in the pH range 7–10, the emission

180   intensity at 521 nm rapidly increases to a maximum. At pH < 6, the enhanced emission does not

181   occur because of protonation of F⁻, preventing fluoride-mediated desilylation.

182   **3.3 Cell imaging**

183   Finally, the potential of the probe **FS** for imaging F⁻ in living cells was investigated. First,

184   an MTT assay with a RAW264.7 cell line was used to determine the cytotoxicity of **FS**. The

185   cellular viability was estimated to be greater than 80% after 24 h, which indicates that **FS** (<30

186   mM) has low cytotoxicity (Fig. 8). Furthermore, images of the cells were obtained using a

187   confocal fluorescence microscope. The cells were then incubated with the chemosensor **FS**

188   (20 µM) for 30 min and then washed with PBS to remove any remaining sensor. Images of the

189   RAW 264.7 cells were obtained by using a confocal fluorescence microscope. Fig. 9 shows

190   images of RAW 264.7 cells with the chemosensor **FS** after treatment with F⁻. An overlay of

191   fluorescence images and bright-field images shows that the fluorescence signals are localized in

192   the intracellular area, indicating subcellular distribution of F⁻ and good cell-membrane

193   permeability of the chemosensor **FS**.

194

195   **4. Conclusion**

196   In conclusion, we have reported a coumarin-based fluorescent chemosensor **FS** for F⁻

197   sensing that exhibits a turn-on response both in vitro and in live cells. The detection of F⁻ is

198   achieved through significant fluorescence enhancement resulting from the fluoride-mediated

199   desilylation. This probe displays high selectivity and sensitivity toward F⁻ over other anions in

200 aqueous solutions. Most importantly, the chemosensor **FS** may have application in fluorescence

201 imaging of living cells. This coumarin-based F⁻ chemosensor provides an effective probe for F⁻

202 sensing.

203

Acknowledgements

207 **Supplementary data**

208 ^{1}H and ^{13}C NMR spectra of **FS**, calibration curve of **FS** with F⁻.

209

210

211 **References**

212 1. P. A. Gale, *Chem. Soc. Rev.*, 2010, **39**, 3746-3771.

213 2. C. Caltagirone and P.A. Gale, *Chem. Soc. Rev.*, 2009, **38**, 520-563.

214 3. R. Martínez-Máñez and F. Sancenón, *Chem. Rev.*, 2003, **103**, 4419-4476.

215 4. M. E. Moragues, R. Martinez-Manez and F. Sancenon, *Chem. Soc. Rev.*, 2011, **40**, 2593-2643.

216 5. L. E. Santos-Figueroa, M.E. Moragues, E. Climent, A. Agostini, R. Martinez-Manez and F.

217 Sancenon, *Chem. Soc. Rev.*, 2013, **42**, 3489-3613.

218 6. R. J. Carton, *Fluoride*, 2006, **39**, 163-172.

219 7. M. H. Arhima, O. P. Gulati and S. C. Sharma, *Phytother. Res.*, 2004, **18**, 244-246.

220 8. H. Matsui, M. Morimoto, K. Horimoto and Y. Nishimura, *Toxicol. in Vitro*, 2007, **21**, 1113-

221 1120.

222 9. H. S. Horowitz, *J. Public Health Dent.*, 2003, **63**, 3-8.

223   10. S. Ayoob and A.K. Gupta, *Crit. Rev.Env. Sci. Tec.*, 2006, **36**, 433-487.

224   11. E. Bassin, D. Wypij, R. Davis and M. Mittleman, *Cancer Causes Control*, 2006, **17**, 421-428.

225   12. M. A. G. T. van den Hoop, R. F. M. J. Cleven, J. J. van Staden and J. Neele, *J. Chromatogr.*

226   *A*, 1996, **739**, 241-248.

227   13. R. I. Stefan, J. F. van Staden and H. Y. Aboul-Enein, Pharm. *Acta Helv.*, 1999, **73**, 307-310.

228   14. R. De Marco, G. Clarke and B. Pejcic, *Electroanal.*, 2007, **19**, 1987-2001.

229   15. W. D. Armstrong, *J. Am. Chem. Soc.*, 1933, **55**, 1741–1742.

230   16. Y. Qu, J. Hua and H. Tian, *Org. Lett.*, 2010, 12, 3320-3323.

231   17. M. Vázquez, L. Fabbrizzi, A. Taglietti, R.M. Pedrido, A.M. González-Noya and M. R.

232   Bermejo, *Angew. Chem. Int. Ed.*, 2004, **43**, 1962-1965.

233   18. K. J. Chang, D. Moon, M.S. Lah and K.S. Jeong, *Angew. Chem. Int. Ed.*, 2005, **44**, 7926-

234   7929.

235   19. M. Boiocchi, L. Del Boca, D. E. Gómez, L. Fabbrizzi, M. Licchelli and E. Monzani, *J. Am.*

236   *Chem. Soc.*, 2004, **126**, 16507-16514.

237   20. A. S. F. Farinha, M. R.C. Fernandes and A. C. Tomé, *Sens. Actuators B*, 2014, **200**, 332–338

238   21. B. Deka and R. J. Sarma, *Sens. Actuators B*, 2014, **197**, 321–325.

239   22. U. N. Yadav, P. Pant, D. Sharma, S. K. Sahoo and G. S. Shankarling, *Sens. Actuators B*,

240   2014, **197**, 73–80.

241   23. V. Luxami, A. S. Gupta and K. Paul, *New J. Chem.,* 2014, **38**, 2841—2846.

242   24. R. Liu, Y. Gao, Q. Zhang, X. Yang, X. Lu, Z. Ke, W. Zhou and J. Qu, *New J. Chem.,* 2014,

243   **38**, 2941—2945.

244   25. X. Yong, M. Su, W. Wan, W. You, X. Lu, J. Qu and R. Liu, *New J. Chem.,* 2013, **37**, 1591—

245   1594.

246 26. Madhuprasad, N. Swathi, J. R. Manjunatha, U. K. Das, A. N. Shetty and D. R. Trivedi, *New*

247 *J. Chem.,* 2014, **38**, 1484--1492

248 27. Z. Q. Liu, M. Shi, F. Y. Li, Q. Fang, Z.H. Chen and T. Yi, *Org. Lett.*, 2005, **7**, 5481-5484.

249 28. C.W. Chiu and F.P. Gabbaï, *J. Am. Chem. Soc.*, 2006, **128**, 14248-14249.

250 29. X. Y. Liu, D. R. Bai and S. Wang, *Angew. Chem. Int. Ed.*, 2006, **45**, 5475-4578.

251 30. X. Liu, M. Mao, M. Ren, Y. Tong and Q. Song, *Sens. Actuators B*, 2014, **200**, 317–324.

252 31. R. Hu, J. Feng, D. Hu, S. Wang, S. Li, Y. Li and G. Yang, *Angew. Chem. Int. Ed.*, 2010, **49**,

253 4915-4918.

254 32. J. F. Zhang, C.S. Lim, S. Bhuniya, B. R. Cho and J. S. Kim, *Org. Lett.*, 2011, **13**, 1190-1193.

255 33. P. Sokkalingam and C.H. Lee, *J. Org. Chem.*, 2011, **76**, 3820-3828.

256 34. B. Zhu, F. Yuan, R. Li, Y. Li, Q. Wei, Z. Ma, B. Du and X. Zhang, *Chem. Commun.*, 2011,

257 **47**, 7098-7100.

258 35. X. Cheng, H. Jia, J. Feng, J. Qin and Z. Li, *Sens. Actuators B*, 2014, **199**, 54-61.

259
260
261
262
263
264
265
266
267
268
269
270

271   **Figure and scheme captions**

272   1. **Scheme 1.** Synthesis of chemosensor **FS**

273   2. **Scheme 2**. The reaction mechanism of **FS** and F⁻.

274   3. **Fig. 1.** Color (top) and fluorescence (bottom) changes in **FS** upon the addition of various
275   anions in a acetonitrile-water (v/v = 1:1, 10 mM Hepes, pH 7.0) solution.

276   4. **Fig. 2.** UV-vis (top) and fluorescence (bottom) spectra of **FS** (10.0 μM) in acetonitrile-water
277   (v/v = 1:1, (C)10 mM Hepes, pH 7.0) solution, after the addition of various anions (1 mM). The
278   excitation wavelength was 465 nm.

279   5. **Fig. 3.** Emission spectra of **FS** (10 μM) in acetonitrile-water (v/v = 1:1, 10 mM Hepes, pH 7.0)
280   solution upon the addition of 0-2 mM of F⁻. The excitation wavelength was 465 nm. The
281   incubation time was 180 minutes.

282   6. **Fig. 4.** Time-course measurement of the fluorescence response of **FS** (10 μM) to F⁻ (1 mM).
283   The excitation wavelength was 465 nm.

284   7. **Fig. 5.** ^{1}H NMR spectral change of the reaction of **FS** with NaF in CDCl$_3$.

285   8. **Fig. 6**. Fluorescence response of chemosensor **FS** (10 μM) to F⁻ (1 mM) or 1 mM of other
286   anions (the black bar portion) and to the mixture of other anions (1 mM) with 1 mM of F⁻ (the
287   gray bar portion) in acetonitrile-water (v/v = 1:1, 10 mM Hepes, pH 7.0) solution

288   9. **Fig. 7.** Fluorescence response of free chemosensor **FS** (10 μM) (▲) and after addition of F⁻ (1
289   mM) (□) in acetonitrile-water (v/v = 1:1, 10 mM buffer, pH 3-4: PBS, pH 4.5-6: MES, pH 6.5-
290   8.5: HEPES, pH 9-10: Tris-HCl) as a function of different pH values. The excitation wavelength
291   was 465 nm.

292   10. **Fig. 8.** Cell viability values (%) estimated by an MTT assay versus incubation concentrations
293   of **FS**. RAW264.7 cells were cultured in the presence of **FS** (0–25 μM) at 37°C for 24 h.

294   11. **Fig. 9.** Fluorescence images of macrophage (RAW 264.7) cells treated with **FS** and NaF.
295   (Left) Bright field image; (Middle) fluorescence image; and (Right) merged image.

296

297

298

299

300

301
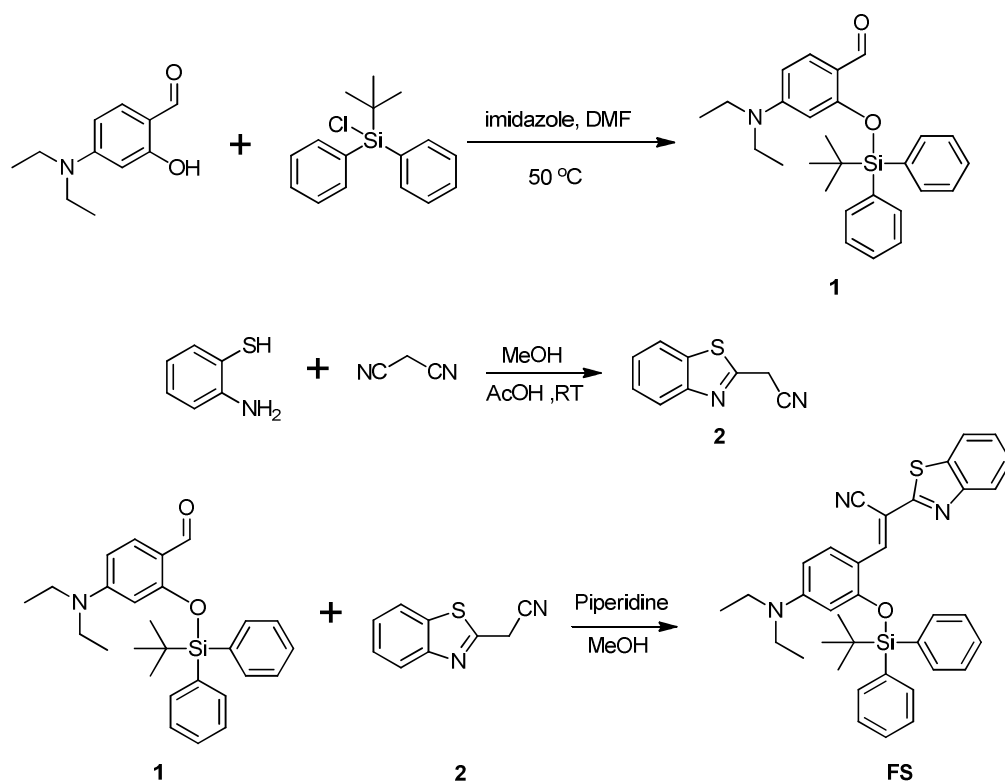
Scheme 1. Synthesis of chemosensor **FS**
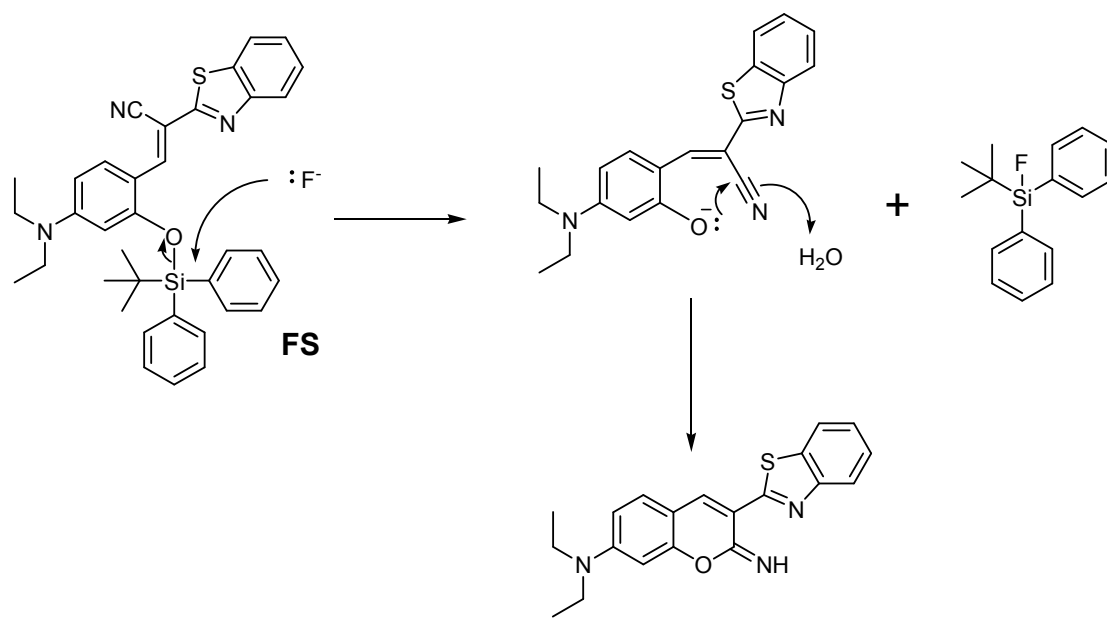
Scheme 2. The reaction mechanism of **FS** and F⁻.
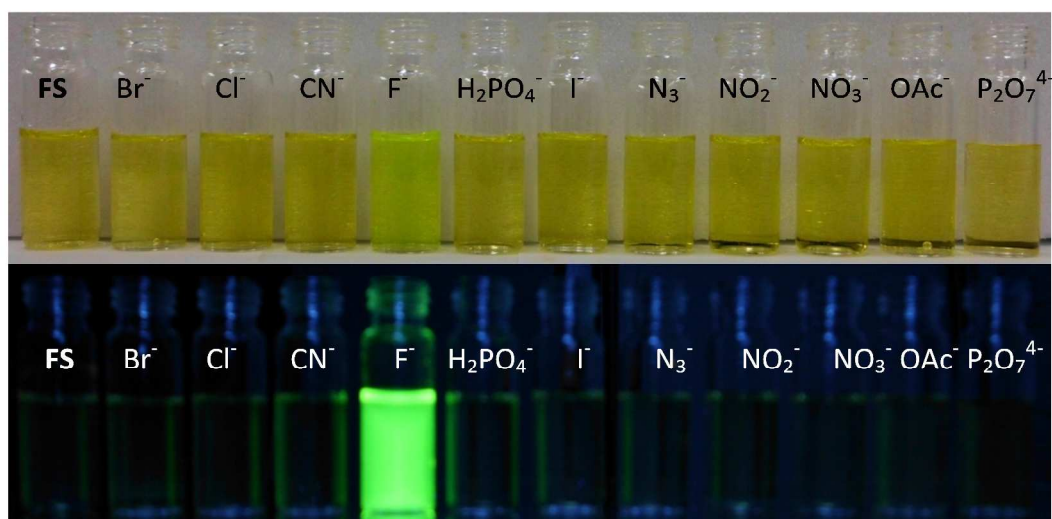
Fig. 1. Color (top) and fluorescence (bottom) changes in **FS** upon the addition of various anions in a acetonitrile-water (v/v = 1:1, 10 mM Hepes, pH 7.0) solution.
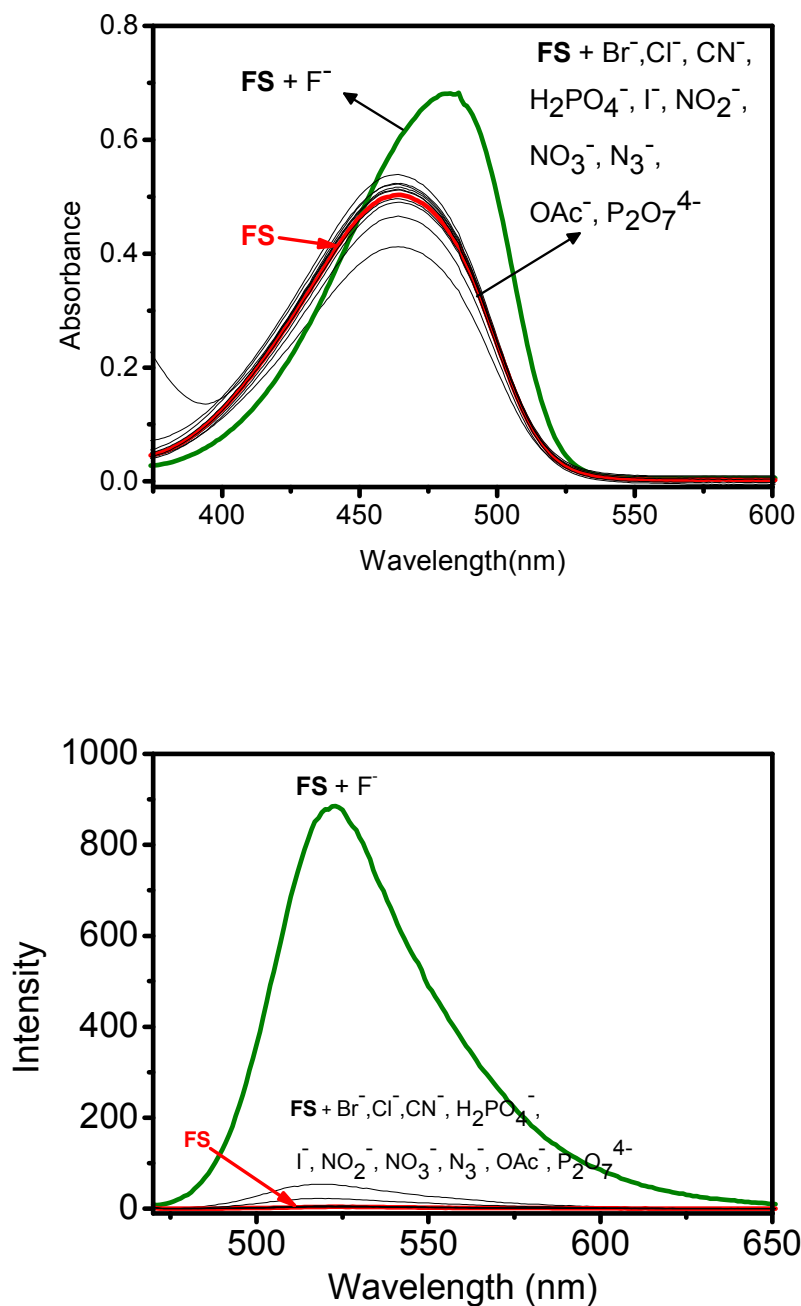
Fig. 2. UV-vis (top) and fluorescence (bottom) spectra of **FS** (10.0 μM) in acetonitrile-water (v/v = 1:1, (C)10 mM Hepes, pH 7.0) solution, after the addition of various anions (1 mM). The excitation wavelength was 465 nm.
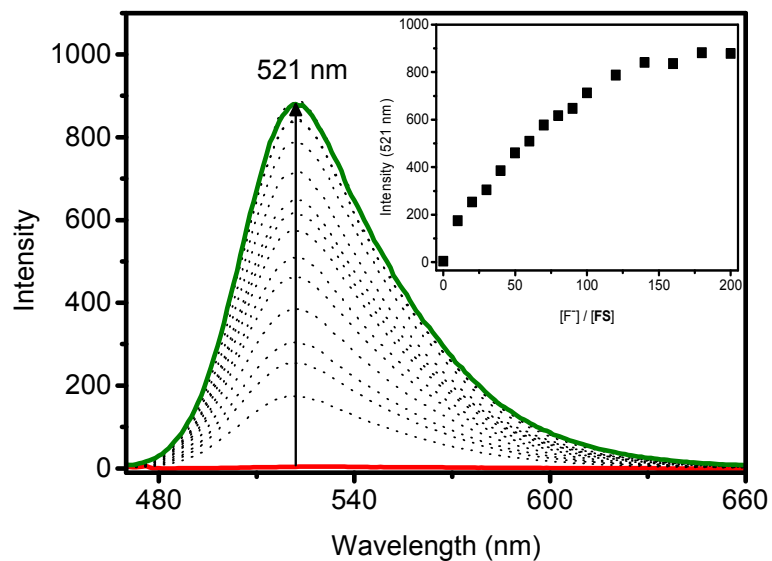
Fig. 3. Emission spectra of **FS** (10 µM) in acetonitrile-water (v/v = 1:1, 10 mM Hepes, pH 7.0) solution upon the addition of 0-2 mM of F⁻. The excitation wavelength was 465 nm. The incubation time was 180 minutes.
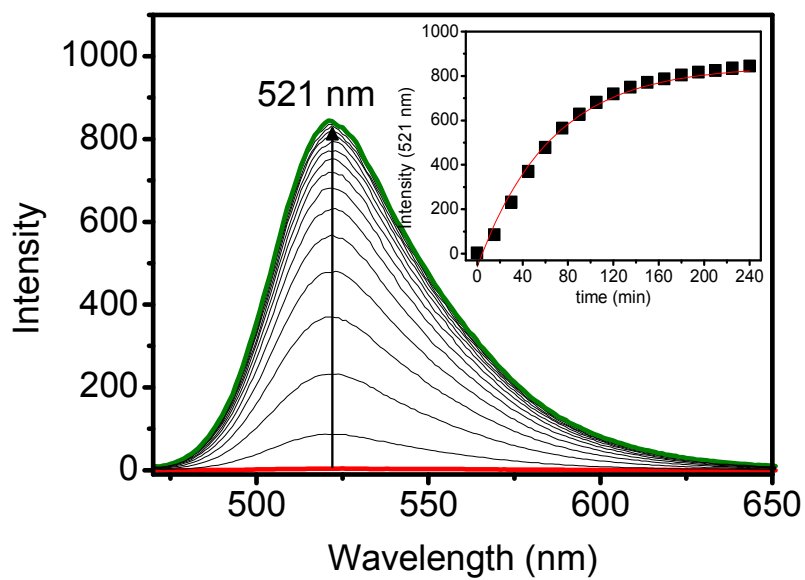
Fig. 4. Time-course measurement of the fluorescence response of **FS** (10 μM) to F⁻ (1 mM). The excitation wavelength was 465 nm.

6
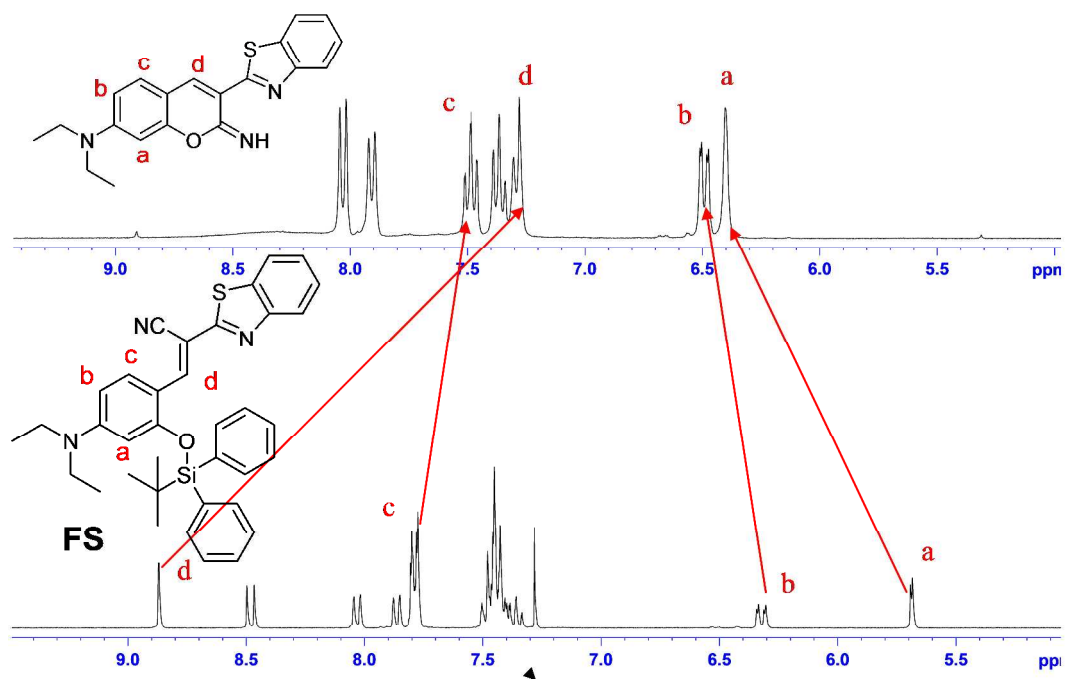
Fig. 5. ^{1}H NMR spectral change of the reaction of **FS** with NaF in CDCl$_3$.
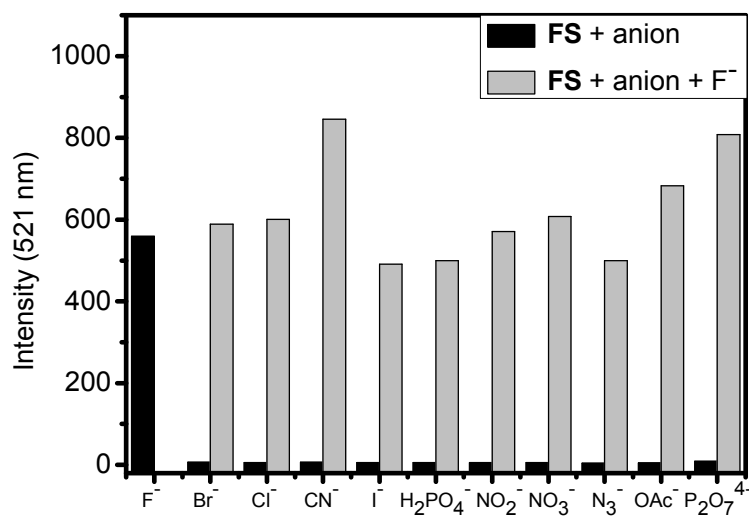
Fig. 6. Fluorescence response of chemosensor **FS** (10 μM) to F$^-$ (1 mM) or 1 mM of other anions (the black bar portion) and to the mixture of other anions (1 mM) with 1 mM of F$^-$ (the gray bar portion) in acetonitrile-water (v/v = 1:1, 10 mM Hepes, pH 7.0) solution
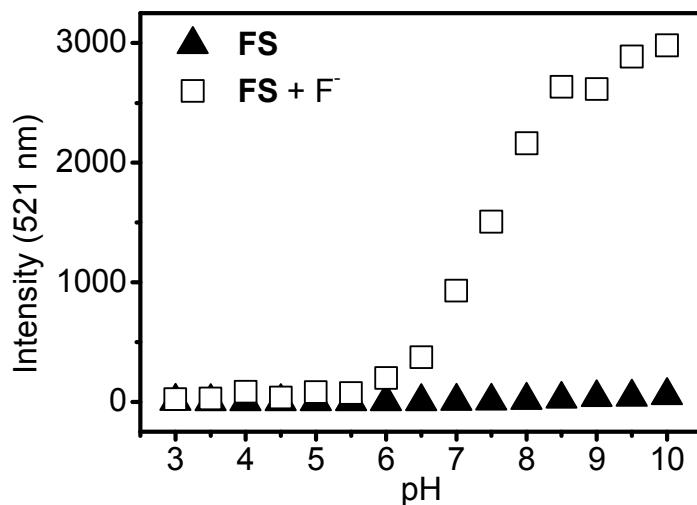
Fig. 7. Fluorescence response of free chemosensor **FS** (10 μM) (▲) and after addition of F⁻ (1 mM) (□) in acetonitrile-water (v/v = 1:1, 10 mM buffer, pH 3-4: PBS, pH 4.5-6: MES, pH 6.5-8.5: HEPES, pH 9-10: Tris-HCl) as a function of different pH values. The excitation wavelength was 465 nm.
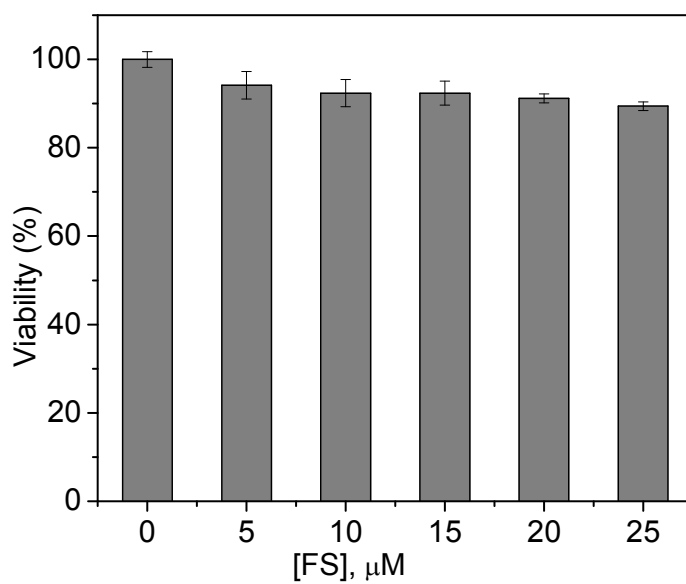
Fig. 8. Cell viability values (%) estimated by an MTT assay versus incubation concentrations of **FS**. RAW264.7 cells were cultured in the presence of **FS** (0–25 µM) at 37°C for 24 h.

Bright field **Fluorescence**
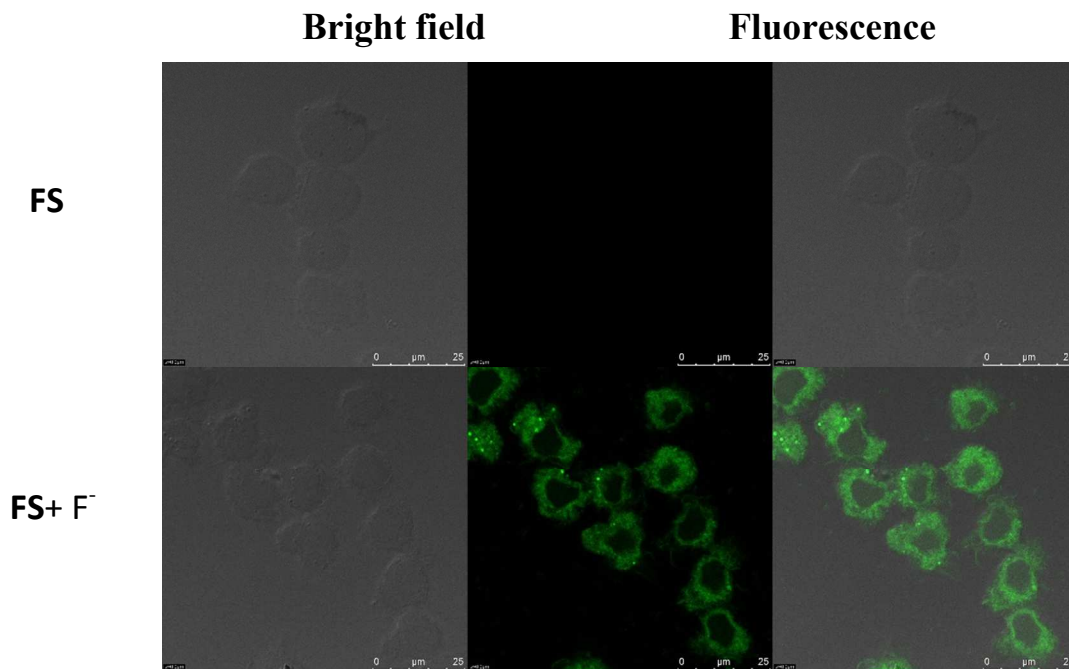
Fig. 9. Fluorescence images of macrophage (RAW 264.7) cells treated with **FS** and NaF. (Left) Bright field image; (Middle) fluorescence image; and (Right) merged image.

A highly sensitive and selective fluorescent probe (**FS**) is based on a fluoride-specific

desilylation reaction to yield significant green fluorescence enhancement.